J. Fluid Mech. (1990), *vol.* 217, *pp.* 547–573
Printed in Great Britain

On the buoyancy-driven motion of a drop towards a rigid surface or a deformable interface

By STERGIOS G. YIANTSIOS AND ROBERT H. DAVIS
Department of Chemical Engineering and Center for Low Gravity Fluid Mechanics and Transport Phenomena, University of Colorado, Boulder, CO 80309-0424, USA

(Received 14 August 1989)

The deformation of a viscous drop, driven by buoyancy towards a solid surface or a deformable interface, is analysed in the asymptotic limit of small Bond number, for which the deformation becomes important only when the drop is close to the solid surface or interface. Lubrication theory is used to describe the flow in the thin gap between the drop and the solid surface or interface, and boundary-integral theory is used in the fluid phases on either side of the gap. The evolution of the drop shape is traced from a relatively undeformed state until a dimple is formed and a long-time quasi-steady-state pattern is established. A wide range of drop to suspending phase viscosity ratios is examined. It is shown that a dimple is always formed, independently of the viscosity ratio, and that the long-time thinning rates take simple forms as inverse fractional powers of time.

1. Introduction

We consider the deformation of a viscous drop, suspended in a surrounding fluid with different properties, as it approaches either a flat rigid surface or a deformable interface. The motion is assumed to be driven by buoyancy and to be sufficiently slow that the creeping equations of motion are valid in all fluid phases involved. Furthermore, the restoring forces due to interfacial tension which resist deformation of the drop from the spherical shape are assumed to be sufficiently strong that the deformation becomes important and alters the behaviour of the system only during the late stages of approach when the gap between the drop and the solid surface or the interface is much smaller than the undeformed drop radius. However, the gap is considered to not have become so small that molecular forces (i.e. of the London/van der Waals type) become important also and cause a relatively fast rupture of the fluid film beneath the drops. Moreover, it is assumed that there are no surfactants on the interfaces which give rise to interfacial-tension gradients or repulsive forces.

The analysis extends the work of Davis, Schonberg & Rallison (1989) who considered the problem of close approach of two spherical drops along their line of centres. Based on the assumption that the gap between the drops is much smaller than both radii, they justified that a lubrication-type flow is established there which dominates the dynamics, and that a large pressure builds up which accounts for the hydrodynamic force resisting the approach of the drops.The simplified hydrodynamics enabled them to obtain simple and accurate expressions for the resistance force as a function of relative velocity for various drop to continuous phase viscosity ratios. As they state, their analysis is valid provided that the constraint $Ca[a/h_0(t)]^2 \ll 1$ or $Ca[a/h_0(t)]^{\frac{3}{2}} \ll 1$, depending on the ratio of viscosities, is satisfied, where $Ca = \mu W/\sigma$ is a capillary number, a the reduced drop radius, $h_0(t)$ the

instantaneous minimum drop separation, μ the drop viscosity, W the relative velocity and σ the interfacial tension. This ensures negligible drop deformation. However, $h_0(t)$ is decreasing with time and therefore at some point the effects of the deformation will become important.

The problem of drop approach and coalescence has been considered by many authors (Hartland 1967, 1969; Hartland & Robinson 1977; Dimitrov & Ivanof 1978; Lin & Slattery 1982). Effects of non-hydrodynamic forces (i.e. of intermolecular and electrostatic origin) have also been incorporated (Chen 1984). Thus it is well known that during the final stages of approach the fluid interfaces take the form of a dimple, underneath which fluid is trapped and draining slowly. However, in these earlier studies, the dimple is assumed already formed and is described in a more or less *ad hoc* manner. Furthermore, *ad hoc* boundary conditions are imposed at the edges of the fluid film beyond the rim of the dimple, and the flow within the drop is not taken into account. Here, we start with the drops being nearly undeformed and trace the evolution of the interfaces until the dimple is formed and the long-time behaviour pattern is established without restorting to *ad hoc* assumptions. We also show that the calculation of the deformation is a singular perturbation problem and requires an outer solution far away from the vicinity of the small gap where lubrication holds. Thus, although the large pressure build-up is restricted to a small region around the drop axis of symmetry, the deformation is of the same order of magnitude everywhere. The outer solution provides the proper boundary conditions to be imposed at the edges of the film, as well as a uniformly valid approximation for the deformation.

As first shown by Frankel & Mysels (1962) and later more completely by Jones & Wilson (1978), at long times after the formation of the dimple the gap thinning rates take simple forms as inverse fractional powers of time. We extend these results by viewing the long-time problem as a perturbation problem, where the small parameter is inverse time, and performing a formal asymptotic analysis. It is shown, in contrast to the statements of Lin & Slattery (1982), that no assumed initial shapes or adjustable parameters are required for the complete description of the film thickness at long times, and moreover that the asymptotic analysis is able to predict the rate at which the dimple radius approaches its final value and consequently the position of the minimum thickness as function of time.

Admittedly, the analysis is restricted to the parameter range of very small capillary numbers in the sense that a lubrication regime has to be established in the gap before any significant deformation occurs, although this still covers a wide range of practical conditions for small drops. Fully numerical calculations over a range of higher capillary numbers have been performed by Chi & Leal (1989), Ascoli (1988) using the boundary-integral method for the solution of the Stokes equations, and by Pozrikidis (1990) who considered also the motion of a drop away from a solid surface. However, these calculations suffer from convergence difficulties at small drop separation distances and thus are not able to reveal the long-time details of the deformation and the rates of thinning. Moreover, Ascoli (1988) states that variation of pressure across the thin gap is a necessary mechanism for the formation of a dimple. In contrast, the analysis presented here shows that dimple formation is possible after a lubrication regime is established in the thin gap.

In §2 we consider the problem of the buoyancy-driven motion of a drop towards a flat rigid surface. We first derive asymptotic expressions for small deformation in the vicinity of the small gap as well as away from it. These are used to provide natural initial and boundary conditions for the numerical calculations, which we

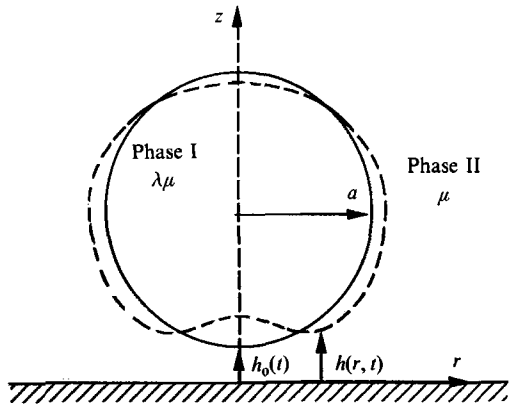

FIGURE 1. Definition sketch for a drop descending towards a flat rigid surface.

extend until the deformation becomes significant, a dimple is formed, and a long-time evolution pattern is established. We also present a long-time asymptotic analysis which extends the results of Jones & Wilson (1978), and the numerical and asymptotic results are compared. Finally, the effect of varying the viscosity ratio is discussed. In §3 the motion of the drop towards a deformable interface is discussed. We first consider the case of a drop much more viscous than the suspending phase, in which case the results from §2 carry over, and then the case of viscosities of the same order of magnitude, where the flow in the gap is coupled with that inside the drop.

2. Drop approaching a flat rigid surface

We consider a viscous incompressible drop of undeformed radius a, viscosity $\lambda\mu$ and density ρ_1, suspended in an unbounded fluid of viscosity μ and density ρ_2, and approaching a flat solid surface. The interface between the two fluids is characterized by constant interfacial tension, σ. For definiteness we assume that $\rho_1 > \rho_2$ and that the wall is underneath the drop as shown in figure 1. Note that figure 1 is a definition sketch and the relevant quantities are not drawn to scale. The case $\rho_2 > \rho_1$ with the wall above the drop is equivalent. We examine first the case $\lambda \gg 1$ in detail, which implies that the drop is much more viscous than the surrounding fluid so that the interface is nearly tangentially immobile. More precise constraints for this to be true are given in §2.5. There we show that the dynamics and the evolution pattern are only slightly affected when the viscosity ratio is reduced.

2.1. *Governing equations* ($\lambda \gg 1$)

We adopt a cylindrical coordinate system with the origin at the intersection of the drop axis of symmetry and the flat wall. The undeformed drop is initially at a distance $h_0 = h_0(0)$ from the wall, where $h_0 \ll a$. Then, as shown by Davis *et al.* (1989), the appropriate lengthscales for changes inside the gap in the z- and r-directions are h_0 and $r_0 = (ah_0)^{\frac{1}{2}}$, respectively. A large pressure builds up in the lubrication area of radius r_0 beneath the drop, which supports the buoyancy force. Hence, the pressure relative to the ambient is $P^{*II} = O(\Delta\rho g a^2/h_0)$, where $\Delta\rho$ is the difference in density between phases I and II, and g is the gravitational acceleration. From the momentum equation in the r-direction, where viscous and pressure forces are in balance, we obtain a radial velocity component, $u^{*II} = O(P^{*II}h_0^2/r_0\mu) =$

$O(\Delta\rho g a^{\frac{3}{2}} h_0^{\frac{1}{2}}/\mu)$. Then, the continuity equation indicates that the normal or axial velocity in the thin gap is $w^{*II} = O(\Delta\rho g a h_0/\mu)$. Inside the drop, both lengthscales are $O(r_0)$, and the balance of shear stresses at the interface suggests that $u^{*I} = O[u^{*II}(r_0/h_0)/\lambda] = O(\Delta\rho g a^2/\lambda\mu)$. From continuity this is also the scale for w^{*I}. The dynamic pressure inside the drop is $P^{*I} = O(u^{*II}\lambda\mu/r_0) = O(\Delta\rho g a^{\frac{3}{2}}/h_0^{\frac{1}{2}})$. Finally, the appropriate timescale is $O(h_0/w^{*II}) = O(\mu/\Delta\rho g a)$.

Using the above scalings for non-dimensionalization, and introducing the modified pressures $\tilde{P}^{*II} = P^{*II} + \rho_2 gz$, $\tilde{P}^{*I} = P^{*I} + \rho_1 gz - 2\sigma/a$ for the continuous phase and the drop, respectively, the creeping equations of motion in the vicinity of the thin gap take the form:

Phase II

$$-\frac{\partial P^{II}}{\partial r} + \frac{\partial^2 u^{II}}{\partial z^2} + \epsilon^2\left[\frac{1}{r}\frac{\partial}{\partial r}\left(r\frac{\partial u^{II}}{\partial r} - \frac{u^{II}}{r^2}\right)\right] = 0, \tag{1a}$$

$$-\frac{\partial P^{II}}{\partial z} + \epsilon^2\frac{\partial^2 w^{II}}{\partial z^2} + \epsilon^4\frac{1}{r}\frac{\partial}{\partial r}\left(r\frac{\partial w^{II}}{\partial r}\right) = 0, \tag{1b}$$

$$\frac{1}{r}\frac{\partial}{\partial r}(ru^{II}) + \frac{\partial w^{II}}{\partial z} = 0. \tag{1c}$$

Phase I

$$-\frac{\partial P^{I}}{\partial r} + \frac{\partial^2 u^{I}}{\partial z^2} + \frac{1}{r}\frac{\partial}{\partial r}\left(r\frac{\partial u^{I}}{\partial r}\right) - \frac{u^{I}}{r^2} = 0, \tag{2a}$$

$$-\frac{\partial P^{I}}{\partial z} + \frac{1}{r}\frac{\partial}{\partial r}\left(r\frac{\partial w^{I}}{\partial r}\right) + \frac{\partial^2 w^{I}}{\partial z^2} = 0, \tag{2b}$$

$$\frac{1}{r}\frac{\partial}{\partial r}(ru^{I}) + \frac{\partial w^{I}}{\partial z} = 0. \tag{2c}$$

The parameter $\epsilon = (h_0/a)^{\frac{1}{2}}$ is small compared with unity. Inertial forces are neglected in both phases, and this requires that the constraints $\rho_1\Delta\rho g a^3/\lambda\mu^2 \ll 1$ and $\rho_2\Delta\rho g a^3/\mu^2 \ll 1$ be imposed.

At the wall we have the no-slip and impenetrability conditions

$$u^{II} = w^{II} = 0 \quad \text{at} \quad z = 0, \tag{3}$$

and at the interface, $z = h(r,t)$, we have the continuity of velocities,

$$u^{II} = u^{I}/\lambda\epsilon, \quad w^{II} = w^{I}/\lambda\epsilon^2, \tag{4}$$

and balance of tangential and normal stresses,

$$\left[1-\epsilon^2\left(\frac{\partial h}{\partial r}\right)^2\right]\left(\frac{\partial u^{II}}{\partial z} + \epsilon^2\frac{\partial w^{II}}{\partial r}\right) + 2\epsilon^2\frac{\partial h}{\partial r}\left(\frac{\partial w^{II}}{\partial z} - \frac{\partial u^{II}}{\partial r}\right)$$
$$= \left[1-\epsilon^2\left(\frac{\partial h}{\partial r}\right)^2\right]\left(\frac{\partial u^{I}}{\partial z} + \frac{\partial w^{I}}{\partial r}\right) + 2\epsilon^2\frac{\partial h}{\partial r}\left(\frac{\partial w^{I}}{\partial z} - \frac{\partial u^{I}}{\partial r}\right). \tag{5a}$$

$$-P^{II}\left[1-\epsilon^2\left(\frac{\partial h}{\partial r}\right)^2\right] + 2\epsilon^2\left[\frac{\partial w^{II}}{\partial z} + \epsilon^2\left(\frac{\partial h}{\partial r}\right)^2\frac{\partial u^{II}}{\partial r} - \frac{\partial h}{\partial r}\left(\frac{\partial u^{II}}{\partial z} + \epsilon\frac{\partial w^{II}}{\partial r}\right)\right]$$
$$+\epsilon P^{I}\left[1-\epsilon^2\left(\frac{\partial h}{\partial r}\right)^2\right] - 2\epsilon\left[\frac{\partial w^{I}}{\partial z} + \epsilon^2\left(\frac{\partial h}{\partial r}\right)^2\frac{\partial u^{I}}{\partial r} - \epsilon\frac{\partial h}{\partial r}\left(\frac{\partial u^{I}}{\partial z} + \frac{\partial w^{I}}{\partial r}\right)\right]$$
$$= \frac{h_0}{aB}\left\{\frac{\partial^2 h}{\partial r^2}\left[1+\epsilon^2\left(\frac{\partial h}{\partial r}\right)^2\right]^{-\frac{1}{2}} + \frac{1}{r}\frac{\partial h}{\partial r}\left[1+\epsilon^2\left(\frac{\partial h}{\partial r}\right)^2\right]^{\frac{1}{2}} - 2\left[1-\epsilon^2\left(\frac{\partial h}{\partial r}\right)^2\right]\right\} + \epsilon^2 h. \tag{5b}$$

Here, $B = \Delta\rho g a^2/\sigma$ is the Bond number. Finally the position of the interface is described by the kinematic boundary condition

$$\frac{\partial h}{\partial t} + u^{\mathrm{II}} \frac{\partial h}{\partial r} = w^{\mathrm{II}}. \tag{6}$$

As can be seen from the normal stress condition (5*b*), the deformation relative to the initial undeformed gap, h_0, is $O(Ba/h_0)$. We define $\delta = Ba/h_0$ for this initial relative deformation scale, and assume that $\epsilon \ll 1$ and $\delta \ll 1$, which of course requires that the Bond number itself must be much smaller than unity. The first condition ensures that a lubrication regime is valid in the thin gap, while the second, which is equivalent to the constraint $Ca(a/h_0)^2$ imposed by Davis *et al.* (1989), ensures that the drop deformation is not important initially. As shown by Davis *et al.* (1989), with $\lambda \gg 1/\epsilon$ the lubrication force resisting the motion of the drop is inversely proportional to the instantaneous gap, h_0, and therefore the gap decreases exponentially (i.e. like e^{-t}) under the action of a constant applied force. Thus the deformation will be small compared with the undeformed gap for a dimensionless time interval shorter than $O[\ln(1/\delta)]$. From the normal stress condition, we also observe that the direct effects of gravity in the gap are negligible, being of $O(Bh_0/a)$.

Given the above constraints, the governing equations (1) yield the following simplified system of equations which describes the evolution of the thin gap as the drop approaches the wall:

$$-\frac{\partial P^{\mathrm{II}}}{\partial r} + \frac{\partial^2 u^{\mathrm{II}}}{\partial z^2} = 0, \tag{7a}$$

$$-\frac{\partial P^{\mathrm{II}}}{\partial z} = 0, \tag{7b}$$

$$\frac{1}{r}\frac{\partial}{\partial r}(r u^{\mathrm{II}}) + \frac{\partial w^{\mathrm{II}}}{\partial z} = 0, \tag{7c}$$

with boundary conditions

$$u^{\mathrm{II}} = 0 \quad \text{at} \quad z = 0 \quad \text{and} \quad z = h(r,t), \tag{8}$$

and

$$-\delta P^{\mathrm{II}} = \frac{1}{r}\frac{\partial}{\partial r}\left(r\frac{\partial h}{\partial r}\right) - 2. \tag{9}$$

which must be supplemented with the kinematic boundary condition (6) and an integral force balance around the drop. The latter takes the form (Davis *et al.* 1989)

$$\int_0^\infty P^{\mathrm{II}} r\,\mathrm{d}r = \tfrac{2}{3}. \tag{10}$$

From (7) we can easily solve for u^{II} and w^{II} in terms of P^{II} which when substituted into (6) yield the well-known lubrication equation:

$$\frac{\partial h}{\partial t} = \frac{1}{12}\frac{1}{r}\frac{\partial}{\partial r}\left(rh^3\frac{\partial P^{\mathrm{II}}}{\partial r}\right). \tag{11}$$

2.2. *Asymptotic solution for small deformation*

We now attempt an asymptotic solution for h and P^{II} for small δ, assuming that they possess simple asymptotic expansions in terms of powers of δ, i.e.

$$h = h_{(0)} + \delta h_{(1)} + \ldots, \quad P^{\mathrm{II}} = P_{(0)} + \delta P_{(1)} + \ldots. \tag{12a, b}$$

At zero order in δ, equations (11) and (9) give

$$\frac{\partial h_{(0)}}{\partial t} = \frac{1}{12}\frac{1}{r}\frac{\partial}{\partial r}\left(r h_{(0)}^3 \frac{\partial P_{(0)}}{\partial r}\right), \tag{13a}$$

$$\frac{1}{r}\frac{\partial}{\partial r}\left[r\frac{\partial h_{(0)}}{\partial r}\right] - 2 = 0, \tag{13b}$$

and at $O(\delta)$

$$\frac{\partial h_{(1)}}{\partial t} = \frac{1}{12r}\frac{\partial}{\partial r}\left(r h_{(0)}^2 \frac{\partial P_{(1)}}{\partial r}\right) + \frac{1}{4r}\frac{\partial}{\partial r}\left(r h_{(0)}^3 h_{(1)} \frac{\partial P_{(0)}}{\partial r}\right), \tag{14a}$$

$$-P_{(0)} = \frac{1}{r}\frac{\partial}{\partial r}\left[r\frac{\partial h_{(1)}}{\partial r}\right]. \tag{14b}$$

From (13b)

$$h_{(0)} = c_0(t) + \tfrac{1}{2}r^2, \tag{15}$$

and from (13a)

$$P_{(0)} = -3\frac{\mathrm{d}c_0}{\mathrm{d}t}(c_0 + \tfrac{1}{2}r^2)^{-2}. \tag{16}$$

Substituing this expression in the integral force balance (10), we obtain

$$-3\frac{\mathrm{d}c_0}{\mathrm{d}t} = \tfrac{2}{3}c_0, \tag{17}$$

from which $c_0 = \mathrm{e}^{-2t/9}$ and

$$h_{(0)} = \mathrm{e}^{-2t/9} + \tfrac{1}{2}r^2, \quad P_{(0)} = \frac{\frac{2}{3}\mathrm{e}^{-2t/9}}{(\mathrm{e}^{-2t/9} + \frac{1}{2}r^2)^2}. \tag{18a, b}$$

Thus, at $O(\delta^0)$ we obtain the evolution of the undeformed gap and the results (apart from a numerical factor due to different scalings) are in agreement with those of Davis *et al.* (1989). Proceeding to $O(\delta)$ we can easily solve for $h_{(1)}$, which represents the small deviation from the spherical shape, finding

$$h_{(1)} = c_1(t) - \tfrac{1}{3}\ln(\mathrm{e}^{-2t/9} + \tfrac{1}{2}r^2). \tag{19}$$

We observe that although the pressure, which causes the drop to deform, decays like r^{-4} away from the axis of symmetry, the same is not true for the deformation which instead diverges like $-\frac{2}{3}\delta \ln r$. This result can be also verified directly by integrating the normal stress condition (9) and using the integral force balance (10), and its physical interpretation is that there is a net external force on the drop from outside the thin gap due to buoyancy. This suggests that we have a singular perturbation problem at hand, and an outer solution for the deformation, which must be of the same order of magnitude, is needed in order to obtain a uniformly valid approximation. However, by using a similar approach to that for the calculation of $c_0, h_{(1)}$ can be completely determined by solving the inner problem only. Hence, the calculation of the outer solution in this case provides only a consistency test on the asymptotics. This is not the case when the drop is approaching a deformable interface where, as will be seen, we need to know the outer solution in order to specify completely the shape of the drop and the interface. For this reason we proceed to find the outer deformation, after determining $c_1(t)$.

We can easily solve (14a) for $P_{(1)}$ to obtain

$$P_{(1)} = -3\frac{\mathrm{d}c_1}{\mathrm{d}t}h_{(0)}^{-2} - \tfrac{4}{3}c_0 c_1 h_{(0)}^{-3} + \tfrac{4}{9}c_0 h_{(0)}^{-3}\ln h_{(0)} + \tfrac{4}{27}c_0 h_{(0)}^{-3} + \frac{\mathrm{d}c_0}{\mathrm{d}t}c_0^{-3}\int_{r^2/2c_0}^{\infty}\frac{\ln(1+\tau)}{\tau(1+\tau)^3}\mathrm{d}\tau. \tag{20a}$$

At $O(\delta)$ the integral force balance (10) gives

$$\int_0^\infty P_{(1)}\, r\, \mathrm{d}r = 0. \tag{20b}$$

This implies that the deformation does not change the total lubrication force exerted on the drop since it must be always equal to the buoyancy force. Performing the integration in (20*b*) we obtain

$$\frac{9}{2}\frac{\mathrm{d}c_1}{\mathrm{d}t} + c_1 + \frac{2t}{27} - \frac{5}{18} = 0. \tag{21}$$

From (21) we can completely specify c_1 provided that an initial condition is given. Such an initial condition could be rigorously obtained by solving for the deformation when the drop is further away from the wall, i.e. when $h_0(t)$ is comparable with the drop radius, a. However, it can be seen from (21) that c_1 approaches the same form,

$$c_1(t) = \frac{5}{18} - \frac{2t}{27}, \tag{22}$$

to within exponentially small terms, independently of the initial condition. Hence, the thicknesss of the gap between the drop and the solid surface becomes to first order in δ

$$h = \mathrm{e}^{-2t/9} + \tfrac{1}{2}r^2 + \delta\left[\frac{5}{18} - \frac{2t}{27} - \frac{1}{3}\ln\left(\mathrm{e}^{-2t/9} + \tfrac{1}{2}r^2\right)\right]. \tag{23}$$

It is interesting to note that the above expression possesses an invariance with respect to the choice of the initial undeformed thickness h_0, as it should. Thus at any instant in time, if h is scaled with the instantaneous undeformed gap $h_0(t)$, r with $[ah_0(t)]^{\frac{1}{2}}$, and provided that δ, which is now redefined as $Ba/h_0(t)$, remains small compared with unity, we have

$$h = 1 + \tfrac{1}{2}r^2 + \delta[\tfrac{5}{18} - \tfrac{1}{3}\ln(1 + \tfrac{1}{2}r^2)]. \tag{24}$$

We now proceed to find the deformation in the outer region away from the vicinity of the gap. The appropriate lengthscale is the radius of the drop, a, while the appropriate velocity scale for the continuous phase is the velocity of approach, $w^{*\mathrm{II}} = O(\Delta\rho g a h_0/\mu)$. Therefore, viscous forces and the dynamic pressure are $O(\Delta\rho g h_0)$ while gravity forces are $O(\Delta\rho g a)$. Consequently viscous forces are unimportant and the deformation in the outer region is caused by gravity forces alone. Thus, the deformation is $O(Ba)$ which is the same as $O(\delta h_0)$, the magnitude of the deformation in the inner region. Of course, the relative deformation is more important in the inner region, since the relevant lengthscale is much smaller there.

The cylindrical coordinate system is not convenient for describing the outer deformation. Instead, we use a system of spherical polar coordinates (R, θ, ϕ) with origin at the centre of the undeformed drop. The position of the interface is then described by $R - f(\theta) = 0$, where

$$f(\theta) = 1 + Bf_1(\theta) + O(B^2) \tag{25}$$

and $f_1(\theta)$ is the deformation in the radial direction. With viscous forces neglected, the deformation in the outer region can be found by applying the normal stress boundary condition, where gravity and capillary forces are the dominant terms. However, the uniform pressure inside the drop will differ from the value in the undeformed state

by an amount of the same order of magnitude as the above forces, in order to account for the incompressibility of the drop. Then the normal stress condition takes the form

$$2-\frac{2}{(f^2+f'^2)^{\frac{1}{2}}}+\frac{\cot\theta f'/f}{(f^2+f'^2)^{\frac{1}{2}}}+\frac{f''f-f'^2}{(f^2+f'^2)^{\frac{3}{2}}}-B(1+f\cos\theta-P^{\mathrm{I}})=0. \tag{26}$$

where the primes denote differentiation with respect to θ. By introducing (25) and changing the independent variable θ to $\chi=\cos\theta$ we obtain

$$\frac{\mathrm{d}}{\mathrm{d}\chi}\left[(1-\chi^2)\frac{\mathrm{d}f_1}{\mathrm{d}\chi}\right]+2f_1-(1+\chi-P^{\mathrm{I}})=0. \tag{27}$$

The two homogeneous solutions of (27) are

$$S_1(\chi)=\chi, \quad S_2(\chi)=F(-\tfrac{1}{2},1,\tfrac{1}{2},\chi^2),$$

where F denotes the hypergeometric function (see Lamb 1932, p. 113) and is logarithmically singular at $\chi=\pm1$. Then, the complete solution can be found to be

$$f_1=[c_2+g(\chi)]S_1+(c_3-\tfrac{1}{2}\chi^2-\tfrac{1}{3}\chi^3)S_2-\tfrac{1}{2}P^{\mathrm{I}}, \tag{28}$$

where $g(\chi)=-\int_0^\chi(1+\chi)S_2(\chi)\,\mathrm{d}\chi$ and is finite at $\chi=\pm1$.

The three unknown constants c_2, c_3, and P^{I} can be determined from the requirements that no singularity exists near $\chi=1$ (the region diametrically opposite to the thin gap) and that the volume of the drop remains unchanged, and from matching with the inner solution. Here, we shall apply only the first requirement which is sufficient to show whether the outer solution has the appropriate form close to the thin gap region. This gives $c_3-\frac{1}{2}\chi^2-\frac{1}{3}\chi^3=0$ at $\chi=1$, or

$$c_3=\tfrac{5}{6} \tag{29}$$

Now, $$S_2\sim-\frac{\Gamma(\frac{1}{2})}{\Gamma(-\frac{1}{2})\Gamma(1)}\ln(1-\chi^2)=\tfrac{1}{2}\ln(1-\chi^2) \quad \text{as} \quad \xi\to-1.$$

Hence, $f_1\sim-\frac{1}{3}\ln(1-\chi^2)$, or, in terms of the inner variable, $f_1\sim\frac{2}{3}\ln r$, which is in agreement with the behaviour of the inner solution for large r. The difference in sign between f_1 and the inner solution (19) is because they refer to different coordinate systems. Volume conservation and matching with the inner solution can be applied in a straightforward manner to give c_2 and P^{I}, but since no information of interest is obtained, this is not done here.

2.3. *Numerical results*

As already stated, the asymptotic results presented in the previous section will be valid for a time interval shorter than $O[\ln(1/\delta)]$, since the undeformed gap decreases exponentially. For longer times, the deformation of the drop interface due to the pressure required to squeeze the fluid out from the narrowing gap is not small compared with the gap thickness. Therefore, in order to obtain the behaviour of the system beyond the small-deformation regime, we must resort to numerical solutions. The system of equations that needs to be solved consists of (9), (10) and (11). The boundary condition

$$h\sim\tfrac{1}{2}r^2-\tfrac{2}{3}\delta\ln r \quad \text{for} \quad r\gg1, \tag{30}$$

which is provided by the asymptotic solution for the outer deformation, is automatically satisfied, as can be verified from (9) and (10).

The numerical approach used is a direct extension of the asymptotic scheme and has been successfully employed for the problem of elastohydrodynamic collisions of

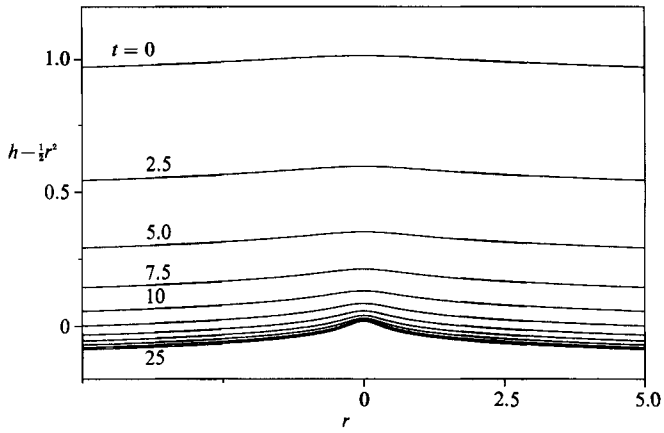

FIGURE 2. The deformation of the drop near the axis of symmetry for short times, with time intervals of $\Delta t = 2.5$. Note that the spherical part, $\frac{1}{2}r^2$, has been subtracted.

solid spheres by Davis, Serayssol & Hinch (1986). More specifically, given the thickness, $h(r,t)$, at a certain instant in time and an initial estimate for the time rate of change, (11) is used to find the pressure in the gap. The magnitude of the rate of change is adjusted so that the calculated pressure satisfies the integral force balance (10). The calculated pressure is then used in (9) to find a new iterate for $h(r,t)$ at the next time step, and the process is repeated until convergence is obtained. Spatial derivatives are approximated using central differences, and time derivatives by backward differences. The spatial domain is from r equal to zero up to a finite value, $r_{\max}$, whch is such that the asymptotic condition (30) is satisfied to within a prescribed tolerance. The contribution to the integral force balance (10) from values of r greater than $r_{\max}$ is calculated analytically by noting that $P \sim r^{-4}$ for large r. As in Davis *et al.* (1986), an adjustable under-relaxation parameter is used in order to improve the convergence characteristics of the numerical scheme. In the numerical calculations, δ is taken to be 0.05, and the asymptotic form (23) with $t = 0$ is used as an initial condition. We note here that if a different choice for the initial gap, h_0, is made then δ, $h(r,t)$ and r have to be rescaled as discussed in the derivation of (24). It might appear that a more straightforward approach would be to calculate the pressure from the normal stress condition and the rate of change of the thickness from the kinematic condition. However, the system of equations is numerically stiff, and this approach would require a prohibitively small time step for convergence.

In figure 2 the shape of the deformation, $h(r,t) - \frac{1}{2}r^2$, is shown for successive time intervals of 2.5, up to time 25. As can be seen, the asymptotic form for large r is established at progressively shorter distances, and the deformation becomes increasingly pronounced in the region close to the drop axis of symmetry, where an increasing curvature opposite to that of the undeformed drop is established.

In figure 3 the total gap thickness, $h(r,t)$, is shown for successive time intervals of 22.5, up to time 119. As can be seen, the drop begins to flatten near the axis of symmetry while the film thinning rate is larger near the edges of the flattened region. This marks the initiation of the formation of the dimple and the trapping of fluid underneath it. Figure 4 shows the evolution of the thickness for time intervals of 180, up to time 1807. As time progresses the film thinning process slows down while the shape of the gap obtains quasi-steady-state features. A minimum occurs at a certain distance from the axis of symmetry which tends slowly towards a steady value of

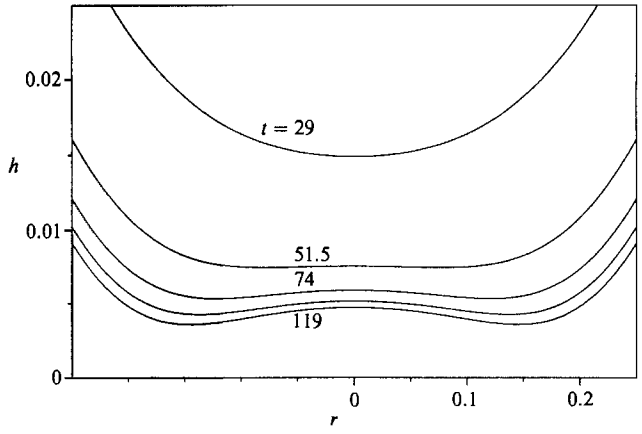

FIGURE 3. The shape of the drop near the axis of symmetry for short times, with time intervals of $\Delta t = 22.5$.

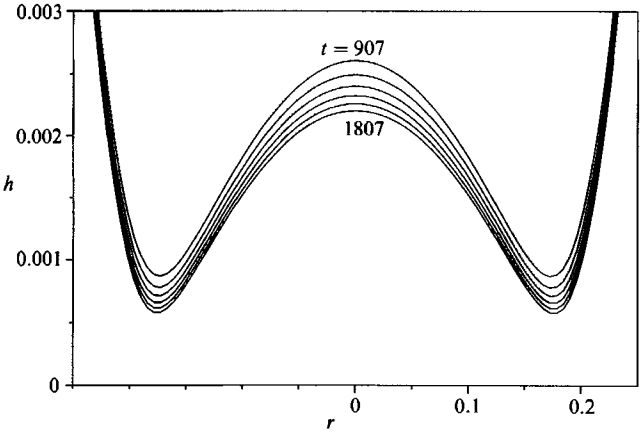

FIGURE 4. The shape of the drop near the axis of symmetry for long times, with time intervals of $\Delta t = 180$.

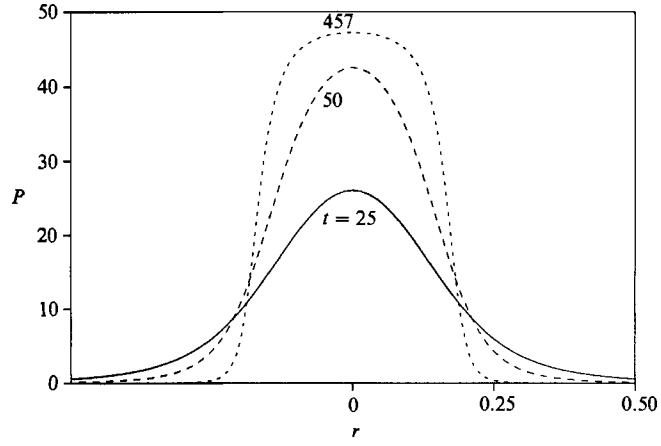

FIGURE 5. The pressure distribution inside the gap for three characteristic times: ——, $t = 25$, when the drop is slightly deformed; – – –, $t = 50$, when the interface is nearly flat; - - -, $t = 457$, when a dimple has been formed.

0.18. The dimple has an approximately parabolic shape with curvature opposite to that of the undeformed sphere. Beyond the dimple, the thickness quickly returns to the asymptotic form given by (30).

In figure 5 the pressure distribution inside the film is shown for three characteristic times. The pressure becomes progressively larger and more concentrated with time, thus causing the interface to flatten. Moreover, the pressure gradient increases with time near the edge of the flattened region, and this induces a relatively faster local thinning rate and the formation of a dimple, until eventually this effect is balanced by the increased local resistance to the outflow. At long times, the pressure inside the dimple (relative to the ambient) is nearly uniform and drops fast beyond its edge. This confirms that the dimple has a parabolic shape to a first approximation. Moreover, it suggests a simple way to calculate the radius of the rim. The pressure inside the dimple is nearly equal to the pressure in the drop, $2\sigma/a$, and balances the buoyancy force. This is true since, as can be seen from figure 4, the slope inside the dimple is smaller than $O(0.01\epsilon)$ and hence the interface is nearly flat. Thus, $(2\sigma/a)(\pi r_{\mathrm{D}}^{*2}) = \frac{4}{3}\pi\Delta\rho g a^3$ from which the dimensional rim radius is

$$r_{\mathrm{D}}^{*} = (\tfrac{2}{3}B)^{\frac{1}{2}}a, \tag{31}$$

or $r_{\mathrm{D}} = (\frac{2}{3}\delta)^{\frac{1}{2}}$. This gives the value 0.1825 for the dimensionless radius of the rim, which is in agreement with the numerical calculations. The result given in (31) was first obtained by Derjaguin & Kussakov (1939).

The fact that the thickness $h(r,t)$ obtains quasi-steady-state features at long times was used by Frankel & Mysels (1962) to predict the long-time thinning rates. A more complete analysis was done independently by Jones & Wilson (1978). They find that for long times the thickness at the drop axis of symmetry decays like $t^{-\frac{1}{4}}$, while that at the edge of the rim like $t^{-\frac{1}{2}}$. Before we compare the numerical results to these predictions we present a formal long-time asymptotic analysis where the small parameter is inverse time. We follow the lines of discussion of Jones & Wilson (1978) and extend their results by showing that the thickness can be completely specified without the need of any assumed initial shapes or adjustable parameters, in contrast to the statements of Lin & Slattery (1982), and by finding the rate at which the rim radius approaches the final value $(\frac{2}{3}B)^{\frac{1}{2}}a$.

2.4. *Long-time asymptotics*

Substituting (9) into (11) we obtain

$$\delta\frac{\partial h}{\partial t} = -\frac{1}{12r}\frac{\partial}{\partial r}\left\{rh^3\frac{\partial}{\partial r}\left[\frac{1}{r}\frac{\partial}{\partial r}\left(r\frac{\partial h}{\partial r}\right)\right]\right\}. \tag{32}$$

We introduce the following rescaling:

$$\tilde{h} = \frac{h}{\delta} = \frac{h^*}{Ba}, \quad \tilde{r} = \frac{r}{(\frac{2}{3}\delta)^{\frac{1}{2}}} = \frac{r^*}{(\frac{2}{3}B)^{-\frac{1}{2}}a},$$

where the asterisks denote the original dimensional variables. Then (32) takes the form

$$\frac{\partial\tilde{h}}{\partial t} = -\frac{3}{16\tilde{r}}\frac{\partial}{\partial\tilde{r}}\left\{\tilde{r}\tilde{h}^3\frac{\partial}{\partial\tilde{r}}\left[\frac{1}{\tilde{r}}\frac{\partial}{\partial\tilde{r}}\left(\tilde{r}\frac{\partial\tilde{h}}{\partial\tilde{r}}\right)\right]\right\}, \tag{33}$$

which is independent of initial conditions.

The spatial domain is divided into three regions: a dimple region I ($0 \leqslant \tilde{r} < 1$), where $\tilde{h} = O(t^{-\frac{1}{4}})$ and the characteristic radial lengthscale is $O(1)$, an outer region

II ($\tilde{r} > 1$) beyond the rim, where $\tilde{h} = O(1)$ and the lengthscale is again $O(1)$, and a rim region III, around $\tilde{r} = 1$, where $\tilde{h} = O(t^{-\frac{1}{2}})$ and the characteristic lengthscale $\hat{r}$ is $O(t^{-\frac{1}{4}})$. We start with the first-order terms and with the asymptotic sequences unspecified. Then by construction it is found that the following expansions for $\tilde{h}$ are valid in the three regions:

$$\tilde{h}_{\mathrm{I}} = t^{-\frac{1}{4}}p_1(\tilde{r}) + t^{-\frac{1}{2}}\ln p_2(\tilde{r}) + t^{-\frac{1}{2}}p_3(\tilde{r}) + t^{-\frac{3}{4}}\ln^2 t p_4(\tilde{r}) + t^{-\frac{3}{4}}\ln t p_5(\tilde{r}) + t^{-\frac{3}{4}}p_6(\tilde{r}) + \ldots, \quad (34a)$$

$$\tilde{h}_{\mathrm{III}} = t^{-\frac{1}{2}}q_1(\hat{r}) + t^{-\frac{3}{4}}q_2(\hat{r}) + \ldots, \quad (34b)$$

$$\tilde{h}_{\mathrm{II}} = s_1(\tilde{r}) + t^{-\frac{1}{2}}s_2(\tilde{r}) + t^{-\frac{3}{4}}s_3(\tilde{r}) + \ldots, \quad (34c)$$

where the inner variable, $\hat{r}$, is defined as

$$\hat{r} = \frac{\tilde{r} - 1 + x(t)}{t^{-\frac{1}{4}}}, \quad \text{with} \quad x(t) = O(t^{-\frac{1}{4}}). \quad (35)$$

Here, $x(t)$ reflects a small uncertainty in the exact position of the inner coordinate which does not affect the leading-order governing equation. Further details are given in the Appendix.

From the asymptotic analysis (see the Appendix) we deduce that the thickness at the drop axis of symmetry decays like $\tilde{h}(0,t) \sim 0.3273t^{-\frac{1}{4}} + 0.0486t^{-\frac{1}{2}}\ln t - 0.6284t^{-\frac{1}{2}}$ or in terms of the original dimensionless variables

$$h(0,t) \sim \delta[0.3273t^{-\frac{1}{4}} + 0.0486t^{-\frac{1}{2}}\ln t - 0.6284t^{-\frac{1}{2}}]. \quad (36)$$

Similarly the minimum thickness at the rim decays like

$$h_{\min}(t) \sim \delta(0.4897)\, t^{-\frac{1}{2}}, \quad (37)$$

and occurs at

$$r_{\mathrm{D}} \sim (\tfrac{2}{3}\delta)^{\frac{1}{2}}(1 - 0.1652t^{-\frac{1}{4}}). \quad (38)$$

In figure 6 (a–c), the numerical calculations for $h(0,t)$, $h_{\min}(t)$, and r_{D} are compared to the asymptotic results. As can be seen, the agreement is good, and this confirms the asymptotic analysis. In figure 6 (a), the result for an undeformed sphere is also shown, which agrees with the numerical results for short times.

From the asymptotic and numerical results presented, a unified picture emerges which describes the behaviour of the drop as it approaches a solid surface. When the drop is far away from the wall it descends with constant velocity given by the Hadamard–Rybczynski formula (Batchelor 1967) and retains a spherical shape independently of the magnitude of interfacial tension. As it approaches at a distance of $O(a)$ from the wall it slows down as described by Wacholder & Weihs (1972), and the redistribution of viscous forces causes a deformation of $O(Ba)$, which is negligible provided that $B \ll 1$. When the drop is at a distance $h_0 \ll a$, a lubrication regime is established in the thin gap between the drop and the solid surface, and the drop descends at an exponentially decreasing rate, provided that $\delta = Ba/h_0 \ll 1$, which implies that the deformation is still negligible. At this point the deformation relative to the instantaneous gap increases, becoming progressively more pronounced and concentrating in a small region of $O(\delta^{\frac{1}{2}})$ around the drop axis of symmetry. When the gap thickness is approximately $0.16Ba$ the interface becomes nearly flat and the higher pressure gradient near the edge of the flattened region induces a faster thinning rate there which results in the formation of a dimple. As time progresses the pressure inside the dimple becomes nearly uniform, the shape of the gap is nearly parabolic, the rim radius tends toward the value $(\frac{2}{3}B)^{\frac{1}{2}}a$, and the evolution features obtain a quasi-steady form. At time infinity the drop becomes flat at its base and the

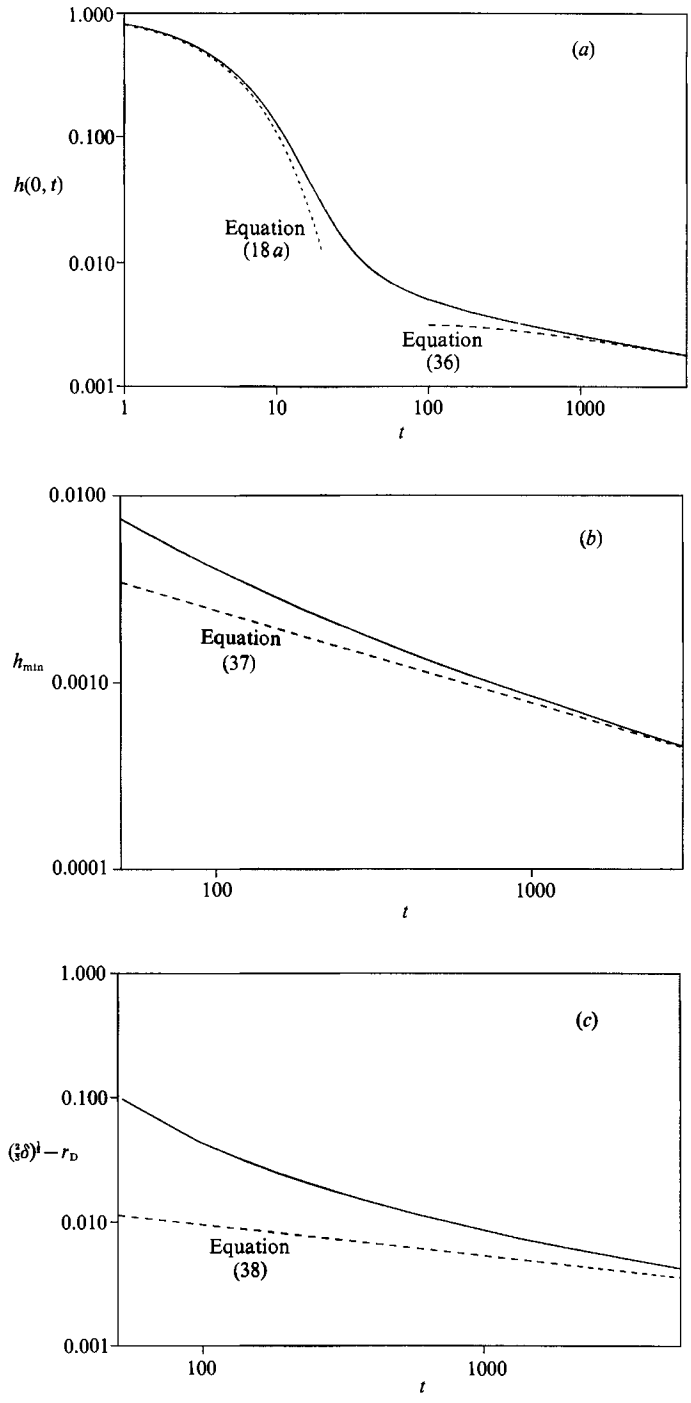

FIGURE 6. Evolution features of the thin gap. (*a*) The thickness at the axis of symmetry: ——, numerical result; ---, short-time asymptotic result for undeformed drop; – – –, long-time asymptotic result for dimpled drop. (*b*) The minimum thickness at the rim: ——, numerical result; ---, long-time asymptotic result. (*c*) The position of the rim relative to the final value, $(\frac{2}{3}\delta)^{\frac{1}{2}}$: ——, numerical result; ---, long-time asymptotic result.

contact angle is zero as can be verified from (A 8). This is so because forces of molecular origin are not incorporated into the analysis and the curvature must be finite everywhere.

2.5. *Effects of the viscosity ratio*

In the analysis presented above we assumed that the drop is much more viscous than the suspending phase so that the tangential mobility of the interface is very small. For this to be true initially, the constraint $\lambda \gg 1/\epsilon$ must be valid. On the other hand, if $\lambda \ll 1/\epsilon$, the interface in the vicinity of the thin gap is almost fully mobile or stress free, and the radial squeeze flow in the gap drives a flow inside the drop with a velocity scale that is of the same order of magnitude as that in the thin film. However, it is easy to verify that equations (9) and (10) remain the same. The analysis for the deformation in the outer region also remains unchanged. In fact, viscous forces are now $O(\Delta\rho g a^{\frac{1}{2}} h_0^{\frac{1}{2}})$ but are still of smaller order of magnitude than gravity and capillary forces. The only difference is that (11) must now be replaced by

$$\frac{\partial h}{\partial t} = \frac{1}{3r}\frac{\partial}{\partial r}\left(rh^3\frac{\partial P^{11}}{\partial r}\right). \tag{39}$$

Therefore, when $\lambda \ll 1/\epsilon$ the same behaviour will manifest itself as the drop approaches the solid surface, but it will simply occur at a pace four times faster. In the intermediate case of $\lambda = O(1/\epsilon)$, the interface is partially mobile and the film drainage and drop flow are fully coupled. The behaviour of the thickness versus time will then be intermediate between the two extremes of tangentially immobile and fully mobile interface. The same conclusions were also reached by Barnocky & Davis (1989), who extended the work of Davis *et al.* (1989) to include the near-contact interaction of spherical drops with rigid and free boundaries and with drops having different properties.

Returning to our original case of a highly viscous drop with initially small tangential mobility of its interface, the initial constraint $\lambda \gg 1/\epsilon = (a/h_0(0))^{\frac{1}{2}}$ must be replaced by the more severe one $\lambda \gg (a/h_0(t))^{\frac{1}{2}}$ as time progresses and the gap thickness decreases. This implies that $\lambda \gg B^{-\frac{1}{3}}$ is required if the drop interface is to be tangentially immobile when the deformation first becomes significant. Finally, when the dimple has formed the proper constraint becomes $\lambda \gg [B\tilde{h}_{\min}(t)]^{-\frac{1}{2}} = O(B^{-\frac{1}{2}}t^{\frac{1}{4}})$. Therefore, at some point in time the assumption of small tangential mobility of the interface will break down and a transition will occur towards the regime of a fully mobile interface, since eventually λ will no longer be large compared to $[B\tilde{h}_{\min}(t)]^{-\frac{1}{2}}$. We finally note here that if surfactants are present, the interface will be tangentially immobile independently of the viscosity ratio.

3. Drop approaching a deformable interface

We now consider the case of a drop of fluid I, suspended in fluid II, and descending owing to buoyancy towards an initially flat interface separating phases II and III. In the analysis to follow, phases I and III will be taken to be identical. A definition sketch is given in figure 7. Again it is assumed that interfacial tension is sufficiently strong to prevent any significant deformation until the minimum separation between the drop and the deformable interface is small enough that a lubrication regime is established in the thin gap. This implies again that $\epsilon = h_0/a \ll 1$ and $\delta \equiv Ba/h_0 \ll 1$. Now account has to be taken of the deformation of both the drop and the interface. We first consider the case $\lambda \gg 1/\epsilon$ which means that phase I (as well as phase III) is much more viscous than phase II.

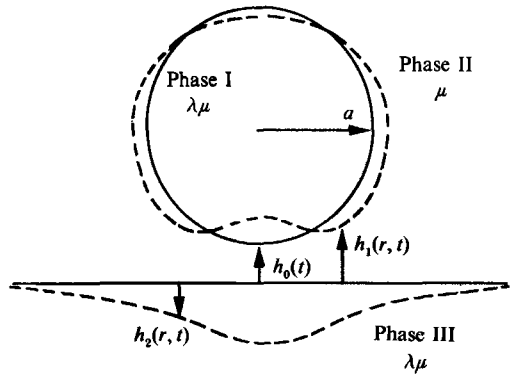

FIGURE 7. Definition sketch for a drop descending towards a deformable interface.

3.1. *The case of small interfacial mobility* ($\lambda \gg 1/\epsilon$)

As before, we adopt a cylindrical coordinate system located at the intersection of the drop axis of symmetry and the undeformed flat interface. The position of the two interfaces near the thin gap is described by $h_1(r,t)$ and $h_2(r,t)$ respectively, while the gap $h(r,t)$ is given by $h = h_1 - h_2$. The same order of magnitude analysis for velocities stresses and pressures applies here as in §2.1. Therefore, in the limit $\epsilon \ll 1$ and $\delta \ll 1$, the governing equations for the thin gap are the same as in (7) while the boundary conditions become

$$u^{\mathrm{II}} = 0 \quad \text{at} \quad z = h_1(r,t) \quad \text{and} \quad h_2(r,t), \tag{40}$$

$$-\delta P^{\mathrm{II}} = \frac{1}{r}\frac{\partial}{\partial r}\left(r\frac{\partial h_1}{\partial r}\right) - 2 \quad \text{at} \quad z = h_1, \tag{41a}$$

$$\delta P^{\mathrm{II}} = \frac{1}{r}\frac{\partial}{\partial r}\left(r\frac{\partial h_2}{\partial r}\right) - 2 \quad \text{at} \quad z = h_2, \tag{41b}$$

and the kinematic boundary conditions at the two interfaces give

$$\frac{\partial h_1}{\partial t} = w^{\mathrm{II}} \quad \text{at} \quad z = h_1, \quad \frac{\partial h_2}{\partial t} = w^{\mathrm{II}} \quad \text{at} \quad z = h_2. \tag{42a, b}$$

Finally, an integral force balance on the drop gives

$$\int_0^\infty P^{\mathrm{II}} r\,\mathrm{d}r = \tfrac{2}{3}. \tag{43}$$

Solving for u^{II} and w^{II} and utilizing the kinematic boundary conditions (42), we obtain the following equation for the gap, $h = h_1 - h_2$:

$$\frac{\partial h}{\partial t} = \frac{1}{12}\frac{1}{r}\frac{\partial}{\partial r}\left(rh^3\frac{\partial P^{\mathrm{II}}}{\partial r}\right). \tag{44}$$

Subtracting (41*b*) from (41*a*) we have

$$-2\delta P^{\mathrm{II}} = \frac{1}{r}\frac{\partial}{\partial r}\left(r\frac{\partial h}{\partial r}\right) - 2. \tag{45}$$

Thus, it is seen that the system of equations (43)–(45) is almost identical to the system (9)–(11) for the case of a drop approaching a solid surface. The only difference

is that δ is now replaced by 2δ. Consequently, the analysis presented in the previous section carries over to this case, and the numerical results shown in figures 2–6 apply here as well, provided that $\delta = 0.025$ rather than $\delta = 0.05$. For long times, a dimple will again be formed whose radial extent will be $r_D = [\frac{2}{3}(2\delta)]^{\frac{1}{2}}$ or in dimensional form

$$r_D^* = (\tfrac{4}{3}B)^{\frac{1}{2}}a. \tag{46}$$

Note that the result given by Jones & Wilson (1978) appears to be in error since the numerical coefficient given is $\frac{1}{12}$ instead of $\frac{4}{3}$.

The only issue that remains to be addressed is how to obtain the deformation of the drop and the interface separately, that is how to obtain h_1 and h_2. Using (41a) and (43) we can easily show that the deformed drop surface is described by

$$h_1 \sim \tfrac{1}{2}r^2 - \tfrac{2}{3}\delta \ln r + O(1) \quad \text{as} \quad r \to \infty. \tag{47}$$

The analysis for the deformation of the drop far away from the gap presented in §2.2 applies here as well an confirms the asymptotic form (47). Now, using (43) and either (41b) or (45), we find that the interface deformation is given by

$$h_2 \sim \tfrac{2}{3}\delta \ln r + O(1) \quad \text{as} \quad r \to \infty. \tag{48}$$

Thus, h_2 like h_1 diverges logarithmically for large r, and an outer solution which eventually decays to zero must be provided in order to obtain a uniformly valid approximation for h_2. The three forces, the balance of which determines the deformation, are gravity, capillary and viscous forces. In the inner region of radial lengthscale $(ah_0)^{\frac{1}{2}}$, gravity is unimportant, and pressure forces cause a deformation of $O(Ba)$. Now, if the outer lengthscale is $O(a)$, capillary forces are $O(\sigma Ba)$, gravity forces are $O(\Delta\rho g Ba)$, and viscous and pressure forces are $O(\Delta\rho g h_0)$. It is easy to verify that capillary forces then dominate over the other two and a homogeneous equation of the form $(1/r)(\partial/\partial r)(r\,\partial h_2/\partial r) = 0$ is obtained. The solution of this equation does not have the appropriate behaviour as $r \to \infty$. Therefore a third lengthscale must exist such that capillary and gravity forces are in balance. This is the capillary length, $(\sigma/\Delta\rho g)^{\frac{1}{2}}$, which is much larger than the drop radius a since $B \ll 1$. Now, if we assume that the velocity field away from the drop decays at least as fast as $1/r$, then viscous and pressure forces are $O(B\Delta\rho g h_0)$ and hence much smaller than capillary and gravity forces. Thus,if we define $r_{(o)} = r^*/(\sigma/\Delta\rho g)^{\frac{1}{2}}$, the appropriate form of the normal stress boundary condition in the outer region becomes

$$\frac{1}{r_{(o)}}\frac{\partial}{\partial r_{(o)}}\left[r_{(o)}\frac{\partial h_2^{(o)}}{\partial r_{(o)}}\right] - h_2^{(o)} = 0. \tag{49}$$

Here, $h_2^{(o)}$ is the deformation of the initially flat interface in the outer region, and is scaled in the same way as the inner gap thickness, h. The solution of (49) which decays to zero as $r_{(o)} \to \infty$ is

$$h_2^{(o)} = cK_0(r_{(o)}), \tag{50}$$

and in fact does so exponentially. Here, K_0 is the modified Bessel function of zero order and the second kind and has the desired logarithmic singularity as $r_{(o)} \to 0$,

$$h_2^{(o)} \sim c(-\ln r_{(o)} + \ln 2 - \gamma), \tag{51}$$

where $\gamma = 0.57721$ is the Euler constant. Rewriting (51) In terms of the inner variable and matching with the inner solution we obtain $c = -\frac{2}{3}\delta$ and

$$h_2 \sim \tfrac{2}{3}\delta(\ln r + \tfrac{1}{2}\ln B\epsilon^2 - \ln 2 + \gamma) \quad \text{as} \quad r \to \infty. \tag{52}$$

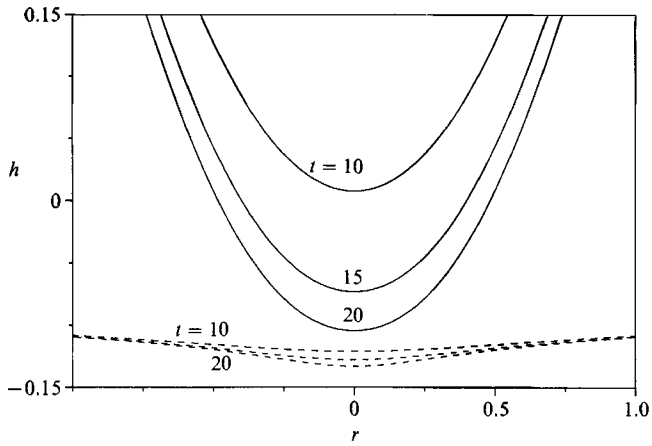

FIGURE 8. The shape of the drop (——) and the interface (– – –) near the axis of symmetry for $\lambda \gg 1$ and short times.

Now, from (41*a*, *b*), it is easy to show that the deformations of the drop and the interface are of similar form:

$$h_1 - \tfrac{1}{2}r^2 = -\delta \int_0^r \frac{1}{\xi} \int_0^\xi P^{\mathrm{II}} \tau \, \mathrm{d}\tau \, \mathrm{d}\xi + c_1(t) = -f(r,t) + c_1(t), \tag{53a}$$

$$h_2 = \delta \int_0^r \frac{1}{\xi} \int_0^\xi P^{\mathrm{II}} \tau \, \mathrm{d}\tau \, \mathrm{d}\xi + c_2(t) = f(r,t) + c_2(t), \tag{53b}$$

from which $f(0,t) = 0$ and $h(r,t) = h_1 - h_2 = \frac{1}{2}r^2 - 2f(r,t) + c_1 + c_2$. Thus

$$h(0,t) = c_1 - c_2. \tag{54}$$

On the other hand, $h(r,t) \sim \frac{1}{2}r^2 - \frac{4}{3}\delta \ln r + c_3(t)$ for $r \gg 1$, where $c_3(t)$ can be found from the numerical calculations at every instant in time. Hence, $f \sim 2\delta/3 \ln r - \frac{1}{2}c_3 + \frac{1}{2}h(0,t)$ as $r \to \infty$, and from (53*b*), $h_2 \sim \frac{2}{3}\delta \ln r - \frac{1}{2}c_3 + \frac{1}{2}h(0,t) + c_2$. Thus, using the asymptotic expression (52) we obtain

$$c_2 + \tfrac{1}{2}(h(0,t) - c_3) = \tfrac{2}{3}\delta(\tfrac{1}{2}\ln B\epsilon^2 - \ln 2 + \gamma), \tag{55}$$

which can be solved together with (54) to give c_1 and c_2 and thus specify h_1 and h_2 completely.

In figures 8 and 9 we show the behaviour of the two interfaces for various characteristic times, with ϵ chosen to be 0.1. As expected, the deformation of the initially flat interface is more pronounced than that of the drop. Note that the negative values of $h_1(r,t)$ indicate that the drop has penetrated the plane representing the initial location of the undeformed interface.

We finally note that if the dimensional interfacial positions, h_1^* and h_2^*, are scaled with Ba, rather than the somewhat arbitrary initial thickness h_0, and r^* with $(\frac{4}{3}B)^{\frac{1}{2}}a$, the asymptotic expression for h_2^* for large r takes the form

$$h_2^* \sim \tfrac{2}{3}Ba(\ln r + \ln B - \tfrac{1}{2}\ln 3 - \gamma). \tag{56}$$

Now, since at time infinity $h^* = 0$ for $r \leqslant 1$ and $h^* = \frac{2}{3}r^2 - \frac{4}{4}\ln r - \frac{2}{3}$ for $r \geqslant 1$, the functions of time $c_1(t)$ and $c_2(t)$ in (53) take the final value $\frac{2}{3}(\ln B) - \frac{1}{3}(\ln 3) - \frac{1}{3} + \frac{2}{3}\gamma$. Hence, in dimensional form

$$h_2^*(0,t) \sim Ba(\tfrac{2}{3}\ln B - \tfrac{1}{3}\ln 3 - \tfrac{1}{3} - \tfrac{2}{3}\gamma), \tag{57}$$

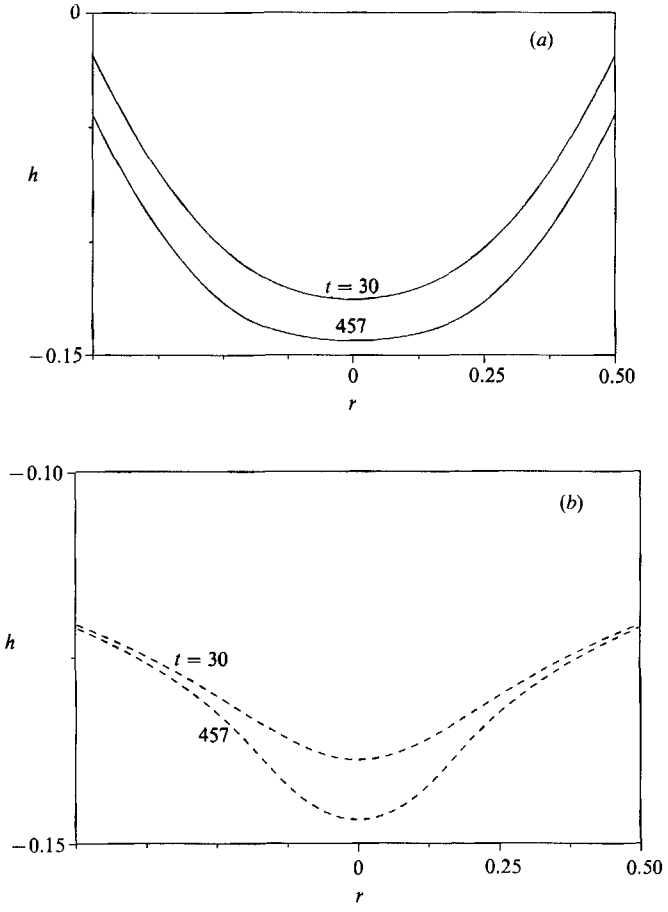

FIGURE 9. Shape of the gap for $\lambda \gg 1$ and two characteristic times: $t = 30$ when the deformation is small, and $t = 457$ when a dimple has formed: (*a*) ——, shape of the drop; (*b*) – – –, shape of the interface.

which is the maximum depression of the initially flat interface at time infinity. Note that the result given by Jones & Wilson (1978) appears to be in error since they give a maximum depression of $O(a)$ (see their equation (A 4)).

3.2. *The case of fully mobile interfaces* ($\epsilon \ll \lambda \ll 1/\epsilon$)

We finally consider the case when the drop (as well as phase III) and the continuous phase II have viscosities of the same order of magnitude. The same constraints as before, namely $\epsilon = (h_0/a)^{\frac{1}{2}} \ll 1$ and $\delta = Ba/h_0 \ll 1$ are imposed. Again, $\delta \ll 1$ is equivalent to the constraint $\lambda Ca(a/h_0)^{\frac{3}{2}} \ll 1$ imposed by Davis *et al.* (1989). The pressure in the gap is $O(\Delta\rho g a^2/h_0)$ which induces a parabolic velocity field u_p^* in the gap of $O(\Delta\rho g a^{\frac{3}{2}} h_0^{\frac{1}{2}}/\mu)$ with associated stresses exerted on the interfaces of $O(\Delta\rho g a^{\frac{3}{2}}/h_0^{\frac{1}{2}})$. Then, the balance of tangential stresses at the interfaces suggests that the velocities inside the drop and phase III are $O(\Delta\rho g a^2/\lambda\mu)$. Continuity of velocities at the interface implies that a uniform radially outward flow exists in the gap with $u^{*II} = O(\Delta\rho g a^2/\lambda\mu)$, which is much larger than u_p^*. Then from the continuity equation we obtain that the normal velocity in the gap, w^{*II}, is $(O(\Delta\rho g a^{\frac{3}{2}} h_0^{\frac{1}{2}}/\lambda\mu)$. Finally, the

timescale is $O(\lambda\mu h_0^{\frac{1}{3}}/\Delta\rho g a^{\frac{3}{2}})$. Using these scalings, the dimensionless governing equations inside the gap take the form

$$-(\lambda\epsilon)\frac{\partial P^{\mathrm{II}}}{\partial r}+\frac{\partial^2 u^{\mathrm{II}}}{\partial z^2}+O(\epsilon^2)=0, \tag{58a}$$

$$-\frac{\partial P^{\mathrm{II}}}{\partial z}=O(\epsilon/\lambda), \tag{58b}$$

$$\frac{1}{r}\frac{\partial}{\partial r}(ru^{\mathrm{II}})+\frac{\partial w^{\mathrm{II}}}{\partial z}=0, \tag{58c}$$

while the full Stokes equations hold inside the drop and in phase III. At the two interfaces, $z=h_1(r,t)$ and $z=h_2(r,t)$, the velocities are continuous:

$$u^{\mathrm{II}}=u^{\mathrm{I}}, \qquad w^{\mathrm{I}}=O(\epsilon) \quad \text{at} \quad z=h_1, \tag{59a}$$

$$u^{\mathrm{II}}=u^{\mathrm{III}}, \quad w^{\mathrm{III}}=O(\epsilon) \quad \text{at} \quad z=h_2. \tag{59b}$$

The shear stress conditions at the two interfaces simplify to

$$\frac{\partial u^{\mathrm{II}}}{\partial z}=\lambda\epsilon\left(\frac{\partial u^{\mathrm{I}}}{\partial z}+\frac{\partial w^{\mathrm{I}}}{\partial r}\right), \quad \frac{\partial u^{\mathrm{II}}}{\partial z}=\lambda\epsilon\left(\frac{\partial u^{\mathrm{III}}}{\partial z}+\frac{\partial w^{\mathrm{III}}}{\partial r}\right) \tag{60a, b}$$

and the normal stress conditions give

$$-\delta P^{\mathrm{II}}=\frac{1}{r}\frac{\partial}{\partial r}\left(r\frac{\partial h_1}{\partial r}\right)-2, \quad \delta P^{\mathrm{II}}=\frac{1}{r}\frac{\partial}{\partial r}\left(r\frac{\partial h_2}{\partial r}\right). \tag{61a, b}$$

Finally, the kinematic boundary conditions at the two interfaces are

$$\frac{\partial h_1}{\partial t}+u^{\mathrm{II}}\frac{\partial h_1}{\partial r}=w^{\mathrm{I}} \quad \text{at} \quad z=h_1, \tag{62a}$$

$$\frac{\partial h_2}{\partial t}+u^{\mathrm{II}}\frac{\partial h_2}{\partial r}=w^{\mathrm{II}} \quad \text{at} \quad z=h_2. \tag{62b}$$

We observe that the problem for flow in the gap is now coupled with that inside the drop and in phase III, and a simultaneous solution is required in order to obtain the evolution of the thin gap in time. From (58*a*) and the tangential stress conditions (60) it is easy to verify that u^{II} is independent of z. Then, using the continuity equation we can solve for w^{II} in terms of u^{II}. Utilizing the two kinematic conditions we obtain the following evolution equation for the thin gap:

$$\frac{\partial h}{\partial t}+\frac{1}{r}\frac{\partial}{\partial r}(ru^{\mathrm{II}}h)=0. \tag{63}$$

Here, $h=h_1-h_2$ as before. The fact that the positions of the two interfaces are unknown complicates the application of the interfacial conditions of continuity of velocities. However, as discussed in Davis *et al.* (1989), since the velocity fields in the drop and phase III are slowly varying in the z-direction, it is permissible to assume that the interfaces are nearly flat. Then an expression for interfacial velocity in terms

of interfacial stress or vice versa can be obtained using boundary-integral theory, and we have (Davis *et al.* 1989, with an error of a factor of 2 corrected)

$$f_t(r) = 4\int_0^\infty \phi(r',r)\left(\frac{u^{\mathrm{II}}}{r'^2} - \frac{1}{r'}\frac{\mathrm{d}u^{\mathrm{II}}}{\mathrm{d}r'} - \frac{\mathrm{d}^2u^{\mathrm{II}}}{\mathrm{d}r'^2}\right)\mathrm{d}r', \tag{64}$$

where

$$\phi(r,r') = \frac{1}{2\pi}\frac{r'}{(r^2+r'^2)^{\frac{1}{2}}}\int_0^\pi \frac{\cos\theta\,\mathrm{d}\theta}{(1-k^2\cos\theta)^{\frac{1}{2}}},$$

is an elliptic-type Green's function kernel, and $k^2 = 2rr'/(r^2+r'^2)$.

The shear stress f_t corresponds to the $O(\lambda\epsilon)$ correction to the uniform flow in the gap and is related to the pressure by

$$f_t = -\frac{\partial P^{\mathrm{II}}}{\partial r}\frac{h}{2}, \tag{65}$$

as can be verified from (58) and (60). Finally, subtracting the two normal stress conditions we obtain a relation between the pressure and the thickness of the gap:

$$-2\delta P^{\mathrm{II}} = \frac{1}{r}\frac{\partial}{\partial r}\left(r\frac{\partial h}{\partial r}\right) - 2, \tag{66}$$

and the problem is closed by writing the integral force balance as before:

$$\int_0^\infty P^{\mathrm{II}} r\,\mathrm{d}r = \tfrac{2}{3}. \tag{67}$$

We note again that $h \sim \frac{1}{2}r^2 - \frac{4}{3}\delta\ln r$ as $r\to\infty$, as can be verified from (66) and (67).

The system of equations (63)–(66) subject to the condition (67) can be solved numerically for the four unknowns (thickness, velocity, interfacial stress and pressure) by a similar approach as before. Given the instantaneous thickness and an initial estimate for its rate of change, u^{II} is calculated from (63). Then f_t is obtained from (64) and P^{II} from (65). The magnitude of the rate of change is adjusted so that (67) is satisfied. Then the calculated pressure is used in (66) to find a new iterate for h at the next time step, and the process is repeated until convergence is obtained. The integrations are performed using Gaussian quadratures. We note that the Green's function kernel $\phi(r,r')$ has an integrable (logarithmic) singularity at $r = r'$. As is the usual procedure with boundary-integral calculations, the singular part is subtracted and calculated analytically.

To obtain the positions of the two interfaces, h_1 and h_2, the same approach as in the previous section is used. For this case, viscous forces at distances of $O(a)$ from the thin gap are $O(\Delta\rho g a^{\frac{1}{2}}h_0^{\frac{1}{2}})$, but this does not affect the analysis and the conclusions drawn there.

In figures 10 and 11 the shape of the two interfaces is shown for various characteristic times for $\delta = 0.025$ and $\epsilon = 0.1$. Again, it can be seen that the deformation of the initially flat interface is more pronounced than that of the drop. Eventually, as can be seen from figure 11, a dimple is formed which has a radius of $(\frac{4}{3}\delta)^{\frac{1}{2}}$, or $(\frac{4}{3}B)^{\frac{1}{2}}a$ in dimensional form, which does not involve the initial conditions. Note, however, that the onset of the formation of the dimple is here delayed compared to the case of nearly rigid interfaces (cf. figure 3) and appears when the thickness at the axis of symmetry has decreased by three orders of magnitude. This explains why Chi & Leal (1989) were unable to detect the formation of the dimple for $\lambda = O(1)$ using the full boundary-integral method.

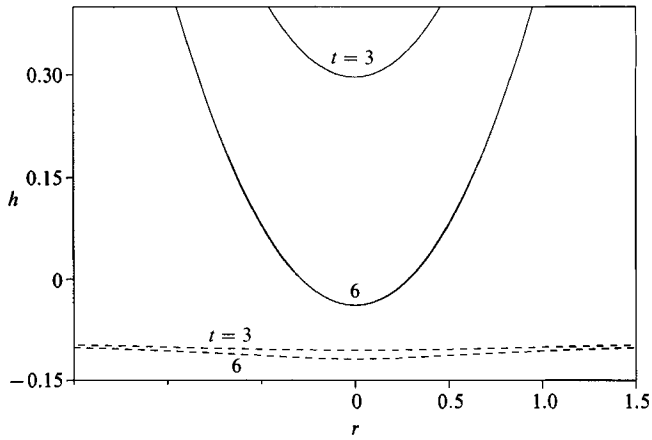

FIGURE 10. The shape of the drop (——) and the interface (– – –) near the axis of symmetry for $\lambda = O(1)$ and short times.

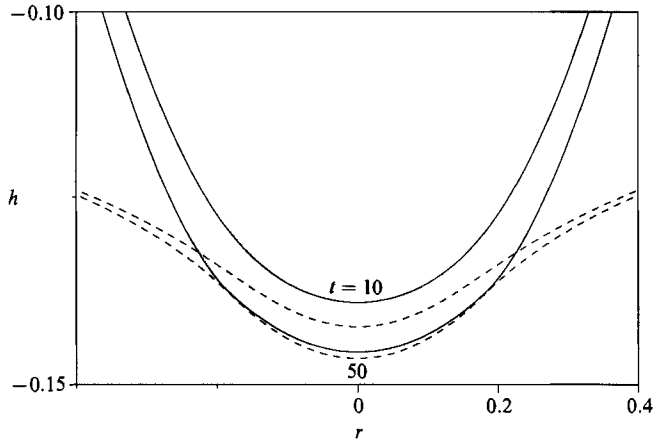

FIGURE 11. Shape of the drop (——) and the interface (– – –) for $\lambda = O(1)$ and two characteristic times: $t = 10$ and $t = 50$.

In figure 12 the behaviour of the thickness $h(0, t)$ at the axis of symmetry is shown as function of time. Also shown is the prediction of Davis *et al.* (1989) for undeformed drops. As they show, undeformed drops with $\lambda = O(1)$ coalesce in a finite time since the lubrication force is inversely proportional to the square root of the instantaneous minimum gap thickness. From their equation (16) we find

$$h_0(t) = (1-0.1269t)^2, \tag{68}$$

and thus coalescence occurs at $t = 7.88$. In contrast, when deformation is taken into account, the mode of approach is not only quantitatively but also qualitatively different since now it takes an infinite time for coalescence to occur (unless an attractive force of molecular origin is also present which increases in magnitude as the gap decreases).

A long-time evolution pattern becomes established eventually, as can be seen for figure 12. Given that now the timescale is much shorter than in the case of nearly rigid interfaces, the film drainage occurs much more quickly, which is not surprising since the two interfaces now offer little resistance to radial outflow. The key steps to

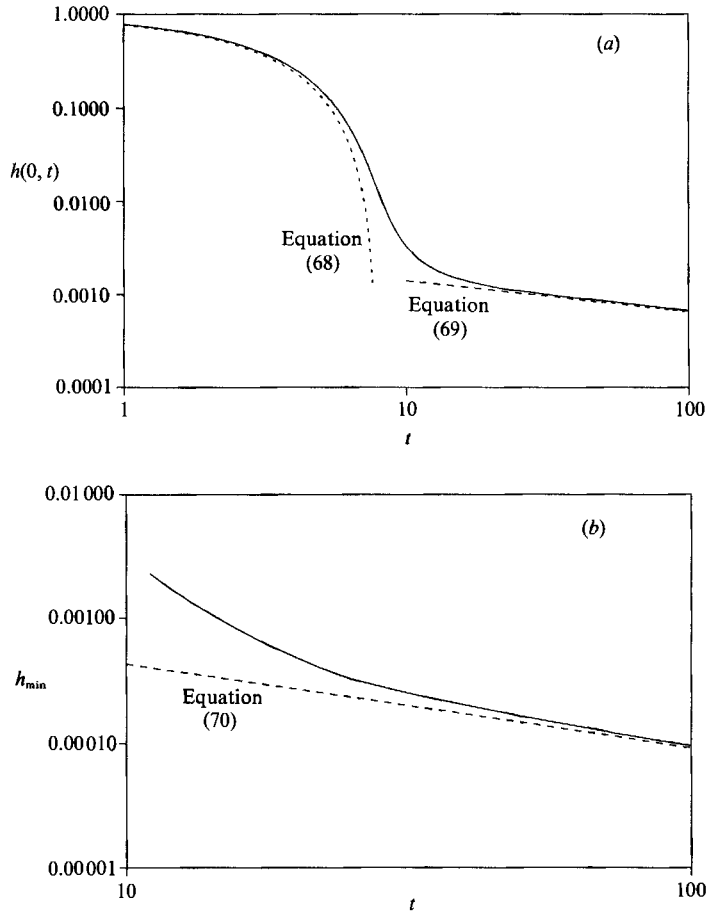

FIGURE 12. Evolution features of the thin gap. (*a*) The thickness at the axis of symmetry, $h(0,t)$, as function of time: ——, numerical result; ---, result for undeformed drop (Davis *et al.* 1989); – – –, asymptotic form proportional to $t^{-\frac{1}{3}}$ for long-times. (*b*) The minimum thickness as function of time: ——, numerical result; ---, asymptotic form proportional to $t^{-\frac{2}{3}}$ for long times.

a long-time asymptotic analysis are similar to those discussed in §2.4, and this problem has also been considered by Jones & Wilson (1978). However, the inner region near the edge of the dimple is described by a nonlinear integro-differential equation and, as they state, there is no prospect of finding an analytical or numerical solution. Thus, quantitative comparisons with the numerical results cannot be made. But their analysis indicates that now the thickness at the axis of symmetry decays like $t^{-\frac{1}{3}}$ and the minimum thickness like $t^{-\frac{2}{3}}$. As can be seen from figure 12, our numerical results agree with this prediction and therefore the numerical analysis is complete and can provide an estimate for the long-time thinning rate. A visual best fit for the long-time thinning rate is shown along with the numerical results, from which we estimate

$$h(0,t) \sim 0.12\delta t^{-\frac{1}{3}}, \tag{69}$$

$$h_{\min} \sim 0.08\delta t^{-\frac{2}{3}}, \tag{70}$$

We finally note that comments similar to those in §2.5 regarding the effect of the viscosity ratio apply here. More specifically, the initial constraint $\lambda \gg 1/\epsilon$, for the

increases to be tangentially immobile, must be replaced by $\lambda \gg B^{-\frac{1}{2}}$ when the deformation becomes significant, and by $\lambda \gg (B\tilde{h}_{\min})^{-\frac{1}{2}}$ when a dimple has been formed. Thus for fixed $\lambda \gg 1$, a transition will occur at some point in time from the regime of nearly tangentially immobile to fully mobile interfaces. Similarly, when $\lambda = O(1/\epsilon)$, a transition will occur from the initial regime of partially mobile increases, in which the flows in the three phases are fully coupled, to the regime of fully mobile interfaces. When $\lambda \leqslant O(\epsilon)$ the lubrication approximation does not apply initially, and the analysis presented here is not valid (Davis *et al.* 1989). However, at some point in time when the gap thickness has decreased sufficiently, the lubrication approximation will become valid, and eventually the film will behave as described in §3.2.

4. Concluding remarks

The rate of approach and the time evolution of the shape of viscous drops driven by buoyancy towards a flat rigid surface or a deformable interface have been analysed under the constraint of small Bond number, $B \equiv (\Delta\rho g a^2/\sigma)$. This constraint ensures that capillary forces prevent any significant deformation until the minimum separation distance is much smaller than the drop radius and a lubrication regime is established in the thin gap. For a typical two-phase system where water is one of the components, the constraints of small Bond and Reynolds number, which must be imposed for the analysis to be valid, yield roughly the same upper limit of approximately 10 μm for the diameter of the drop. Non-hydrodynamic forces (i.e. of intermolecular or electrostatic origin) have not been incorporated into the analysis. However, these forces become important for films with thickness of O(10 nm), which could be two or three orders of magnitude smaller than those for which the present analysis holds. Therefore, although the results presented will not be valid for arbitarily long times, they are expected to give a quantitative prediction of the major part of the film thinning history prior to rupture and drop coalescence.

The analysis is free from any *ad hoc* assumptions and is able to predict naturally the evolution of the shape of the drop and the deformable interface near the thin gap, as well as away from it. Account is taken of the flow in all fluid phases involved. It is shown that the absolute deformation is of the same order of magnitude everywhere around the drop, whereas the relative deformation is most important in the near-contact region. The numerical calculations trace the evolution from a relatively undeformed state where the results of Davis *et al.* (1989) hold, until a dimple is formed and a long-time quasi-steady-state pattern is established. It is shown that for sufficiently long times a dimple is always formed, independently of the ratio of viscosities of the drop and the suspending phase. The dimple radius is $(\frac{2}{3}B)^{\frac{1}{2}}a$ and $(\frac{4}{3}B)^{\frac{1}{2}}a$ when the drop approaches a solid surface and a deformable interface, respectively, and in the second case the maximum depression of the interface is $O(B \ln B)$.

This work was supported by NSF grants CBT-8451014 and CTS-8914236, and by NASA grant NAGW-951.

Appendix. Long-time asymptotics for a drop approaching a wall

We first solve for $\tilde{h}_1$. At $O(t^{-\frac{1}{2}})$, substituting (34a) into (33) we obtain

$$\frac{\mathrm{d}}{\mathrm{d}\tilde{r}}\left[\frac{1}{\tilde{r}}\frac{\mathrm{d}}{\mathrm{d}\tilde{r}}\left(\tilde{r}\frac{\mathrm{d}p_1}{\mathrm{d}\tilde{r}}\right)\right]=0, \tag{A 1}$$

from which

$$p_1 = b_1(1-\tilde{r}^2), \tag{A 2}$$

since $\tilde{h}$ must be regular at $\tilde{r}=0$ and is $O(t^{-\frac{1}{2}})$ as $\tilde{r}\to 1$. The constant b_1 will be determined from matching with the rim solution. At $O(t^{-\frac{1}{2}}\ln t)$ we obtain an equation for p_2 which is identical to (A 1) and thus

$$p_2 = b_2+b_3(1-\tilde{r}^2). \tag{A 3}$$

At $O(t^{-\frac{1}{2}})$ transient effects appear in the outer region I and we have

$$-\tfrac{1}{4}p_1 = -\frac{3}{16\tilde{r}}\frac{\mathrm{d}}{\mathrm{d}\tilde{r}}\left\{\tilde{r}p_1^3\frac{\mathrm{d}}{\mathrm{d}\tilde{r}}\left[\frac{1}{\tilde{r}}\frac{\mathrm{d}}{\mathrm{d}\tilde{r}}\left(\tilde{r}\frac{\mathrm{d}p_3}{\mathrm{d}\tilde{r}}\right)\right]\right\}, \tag{A 4}$$

which can be solved for p_3 to give

$$p_3(\tilde{r}) = -\frac{1}{12b_1^2}\int_0^{\tilde{r}}\frac{\ln(1-\tau^2)}{\tau}\,\mathrm{d}\tau-\frac{1}{48b_1^2}\ln(1-\tilde{r}^2)+b_4+b_5(1-\tilde{r}^2). \tag{A 5}$$

At $O(t^{-\frac{3}{4}}\ln t)$ again an equation which is identical to (A 1) is obtained for p_4. Thus

$$p_4 = b_6+b_7(1-\tilde{r}^2). \tag{A 6}$$

Proceeding in the same fashion we can solve for p_5, p_6 in a straightforward manner, although since the algebra becomes tedious, details are omitted.

We now turn to the outer region II, and at $O(1)$ we obtain

$$\frac{\mathrm{d}}{\mathrm{d}\hat{r}}\left[\frac{1}{\hat{r}}\frac{\mathrm{d}}{\mathrm{d}\hat{r}}\left(\hat{r}\frac{\mathrm{d}s_1}{\mathrm{d}\hat{r}}\right)\right]=0. \tag{A 7}$$

The solution to the above equation must match with the outer solution far away from the gap, obtained in §2.2, and also tend to zero as $\tilde{r}\to 1$. Therefore

$$s_1 = \tfrac{1}{3}\hat{r}^2-\tfrac{2}{3}\ln\hat{r}-\tfrac{1}{3}. \tag{A 8}$$

At $O(t^{-\frac{1}{2}})$ an equation identical to (A 7) is obtained for s_2, and thus s_2 must have a form similar to (A 8). But since $\tilde{h}_{\mathrm{II}}\sim\frac{1}{2}\hat{r}^2-\frac{2}{3}\log\hat{r}$ as $\tilde{r}\to\infty$ for all times, as dictated from the outer solution far away from the gap, the quadratic and logarithmic parts are not allowed and s_2 must be a constant. The same is true for s_3.

We finally turn to the rim region in order to determine $\tilde{h}_{\mathrm{III}}$. At $O(t^{-\frac{1}{2}})$ we obtain

$$\frac{\mathrm{d}}{\mathrm{d}\hat{r}}\left(q_1^3\frac{\mathrm{d}^3q_1}{\mathrm{d}\hat{r}^3}\right)=0 \quad\text{or}\quad q_1^3\frac{\mathrm{d}^3q_1}{\mathrm{d}\hat{r}^3}=d_1. \tag{A 9}$$

We rescale q_1 and $\hat{r}$ by defining

$$q_1 = d_2\bar{q}_1, \quad \hat{r}=d_3\bar{r}. \tag{A 10}$$

Then (A 9) takes the form

$$\bar{q}_1\frac{\mathrm{d}^3\bar{q}_1}{\mathrm{d}\bar{r}^3}=1, \tag{A 11}$$

where, for convenience, we have set

$$d_1 d_3^3/d_2^4 = 1. \tag{A 12}$$

Equation (A 11) has been solved numerically by Jones & Wilson (1978) with the boundary condition $\bar{q}_1 \sim -\bar{r}$ as $\bar{r} \to -\infty$. More precisely they found that

$$\bar{q}_1 \sim -\bar{r} - \tfrac{1}{2}\ln(-\bar{r}) - \tfrac{1}{4}\ln(-\bar{r})/\bar{r} + O(1/\bar{r}) \quad \text{as} \quad \bar{r} \to -\infty, \tag{A 13}$$

and also that $\bar{q}_1 \sim \frac{1}{2}(1.2147\bar{r}^2)$ as $\bar{r} \to \infty$, while a minimum of 1.2571 occurs near $\bar{r} = 0$. We repeated the calculation to find more precisely that

$$\bar{q}_1 \sim \tfrac{1}{2}(1.2908\bar{r}^2) - 0.052\bar{r} + O(1) \quad \text{as} \quad \bar{r} \to \infty, \tag{A 14}$$

and that a minimum of 1.2592 occurs at $\bar{r} = -0.236$.

At $O(t^{-\frac{3}{4}})$ we obtain

$$q_1^3 \frac{\mathrm{d}^3 q_2}{\mathrm{d}\hat{r}^3} + 3d_1 \frac{q_2}{q_1} = d_4 - \hat{r}\, d_1 - q_1^3 \frac{\mathrm{d}^2 q_1}{\mathrm{d}\hat{r}^2}, \tag{A 15}$$

which, after rescaling q_1 and $\hat{r}$ as in (A 10) and setting $q_2 = d_2 d_3 \bar{q}_2$, can be written as

$$\bar{q}_1 \frac{\mathrm{d}^3 \bar{q}_2}{\mathrm{d}\bar{r}^3} + 3\frac{\bar{q}_2}{\bar{q}_1} = \frac{d_4 d_3^2}{d_2^4} - \left(\bar{r} + \bar{q}_1^3 \frac{\mathrm{d}^2 \bar{q}_1}{\mathrm{d}\bar{r}^2}\right). \tag{A 16}$$

The solution to the above equation is obtained as a superposition of $\bar{q}_{21} = d_5 \bar{q}_1$, which is a multiple of $\bar{q}_1$ and cancels the constant forcing term $d_4 d_3^2/d_2^4$, and a part $\bar{q}_{22}$ that satisfies the remaining equation. This was found numerically using the asymptotic expansion

$$\bar{q}_{22} \sim -\tfrac{1}{2}\bar{r}^2 - 2\bar{r}\ln(-\bar{r}) + O(1) \quad \text{as} \quad \bar{r} \to -\infty \tag{A 17}$$

as the initial condition, and integrating from large negative values of $\bar{r}$. In this way, we find that

$$\bar{q}_{22} \sim -0.2016\bar{r}^3 + 1.09\bar{r}^2 + O(\bar{r}) \quad \text{as} \quad \bar{r} \to \infty. \tag{A 18}$$

We are now in the position to apply matching in order to obtain the unknown constants. Since $\bar{q}_1$ behaves as shown in (A 14) for $\bar{r} \to \infty$, $x(t)$ must be of the form $x(t) = x_1 t^{-\frac{1}{4}} + O(t^{-\frac{1}{2}})$. Rewriting the outer solution II In terms of the inner variable $\hat{r}$ and expanding for large t we obtain

$$\tilde{h}_{\mathrm{II}} \sim [\tfrac{2}{3}\hat{r}^2 - \tfrac{4}{3}x_1\hat{r} + O(1)]\, t^{-\frac{1}{2}} + [-\tfrac{2}{9}\hat{r}^3 + \tfrac{2}{3}x_1\hat{r}^2 + O(\hat{r})]\, t^{-\frac{3}{4}}. \tag{A 19}$$

The expression for the inner solution as $\hat{r} \to \infty$ takes the form

$$\tilde{h}_{\mathrm{III}} \sim \left[\frac{1.2098 d_2}{2d_3^2}\hat{r}^2 - \frac{0.052 d_2}{d_3}\hat{r} + O(1)\right] t^{-\frac{1}{2}} + \left[-\frac{0.2016 d_2}{d_3^2}\hat{r}^3 + \left(\frac{1.09 d_2}{d_3} + \frac{1.2098 d_2 d_5}{2d_3^2}\right)\hat{r}^2 + O(\hat{r})\right] t^{-\frac{3}{4}}. \tag{A 20}$$

From (A 19) and (A 20) we obtain

$$\frac{1.2098 d_2}{2d_3^2} = \frac{2}{3}; \quad \frac{0.052 d_2}{d_3} = \frac{4x_1}{3}; \quad \frac{0.2016 d_2}{d_3^2} = \frac{2}{9}; \quad \frac{1.09 d_2}{d_3} + \frac{1.2098 d_2 d_5}{d_3^2} = \frac{2x_1}{3}. \tag{A 21 a–d}$$

Similarly, rewriting the outer solution I in terms of the inner variable $\hat{r}$ we obtain

$$\tilde{h}_1 \sim \left[\left(b_2+\frac{1}{192b_1^2}\right)\left(1+\frac{1}{96b_1^3\hat{r}}\right)\right]t^{-\frac{1}{2}}\ln t+\left[-2b_1\hat{r}-\frac{1}{48b_1^2}\ln(-\hat{r})\right.$$
$$\left.+b_4+2b_1x_1+\frac{\pi^2}{144b_1^2}-\frac{\ln 2}{48b_1^2}-\frac{1}{2.48^2b_1^5}\frac{\ln(-\hat{r})}{\hat{r}}+O\left(\frac{1}{\hat{r}}\right)\right]t^{-\frac{1}{2}}$$
$$+[b_6+O(1)]t^{-\frac{3}{4}}\ln^2 t+\left[-2b_3\hat{r}+\frac{1}{48b_1^2}\hat{r}+O(1)\right]t^{-\frac{3}{4}}\ln t$$
$$+\left[-b_1\hat{r}^2-\frac{1}{12b_1^2}\hat{r}\ln(-\hat{r})+\left(-2b_5+2b_1x_1+\frac{1-\ln 2}{12b_1^2}\right)\hat{r}+O(1)\right]t^{-\frac{3}{4}}. \tag{A 22}$$

The expression for the inner solution as $\hat{r}\to-\infty$ takes the form

$$\tilde{h}_{\mathrm{III}} \sim \left[-\frac{d_2}{d_3}\hat{r}-\tfrac{1}{2}d_2\ln(-\hat{r})+\tfrac{1}{2}d_2\ln(d_3)-\tfrac{1}{4}d_2d_3\frac{\ln(-\hat{r})}{\hat{r}}+O(1)\right]t^{-\frac{1}{2}}$$
$$+\left[-\frac{d_2}{2d_3}\hat{r}^2-2d_2\hat{r}\ln(-\hat{r})+\left(-\frac{d_2d_5}{d_3}+2d_2\ln d_3\right)\hat{r}+O(1)\right]t^{-\frac{3}{4}}. \tag{A 23}$$

From (A 22) and (A 23) we obtain a set of algebraic equations, which can be used together with (A 12) and (A 21) to find the coefficients of interest. Some of these equations are redundant, and serve as consistency tests which verify the correctness of the assumed expansions. We have

$$b_2=-\frac{1}{192b_1^2},\quad 2b_1=\frac{d_2}{d_3};\quad \frac{1}{48b_1^2}=\frac{d_2}{2};\quad b_4+2b_1x_1+\frac{\pi^2}{144b^21}-\frac{\ln 2}{48b_1^2}=\tfrac{1}{2}d_2\ln(d_3);$$
$$2b_3=\frac{1}{48b_1^2};\quad -2b_5+2b_1x_1+\frac{1-\ln 2}{12b_1^2}=-\frac{d_2d_5}{d_3}+2d_2\ln(d_3). \tag{A 24a–f}$$

Solving (A 12), (A 21), and (A 24) we obtain

$$b_1=0.3273;\quad b_2=-0.0486;\quad b_3=0.0972;\quad b_4=0.6239;\quad b_5=0.0045,$$
$$d_1=0.1091;\quad d_2=0.3888;\quad d_3=0.5940;\quad d_4=-0.2660;\quad d_5=-1.0260,$$
$$x_1=0.0256.$$

From the above, we can find that the thickness at the axis of symmetry is

$$\tilde{h}(0,t)\sim b_1t^{-\frac{1}{4}}+(b_2+b_3)t^{-\frac{1}{2}}\ln t+(b_4+b_5)t^{-\frac{1}{2}}+\ldots, \tag{A 25}$$

that the minimum thickness is

$$\tilde{h}_{\min}(t)\sim 1.2592d_2t^{-\frac{1}{2}}+\ldots, \tag{A 26}$$

and that the radius of the dimple is

$$\hat{r}\sim 1-(0.236d_3+x_1)t^{-\frac{1}{4}}+\ldots. \tag{A 27}$$

REFERENCES

Ascoli, E. P. 1988 The effects of a planar wall on the low Reynolds number motion of solid particles, drops and bubbles. Ph.D thesis, Cal. Inst. Tech., Pasadena, California.

Barnocky, G. & Davis, R. H. 1989 The lubrication force between spherical drops, bubbles and rigid particles in a viscous fluid. *Intl J. Multiphase Flow* **15**, 627–638.

BATCHELOR, G. K. 1967 *An Introduction to Fluid Dynamics*. Cambridge University Press.

CHEN, J.-D. 1984 Effects of London–van der Waals and electric double layer forces on the thinning of a dimpled film between a soap drop or bubble and a horizontal solid surface. *J. Colloid. Interface Sci.* **98**, 329–341.

CHI, B. K. & LEAL, L. G. 1989 A theoretical study of the motion of a viscous drop towards a fluid interface at low Reynolds numbers. *J. Fluid Mech.* **201**, 123–146.

DAVIS R. H., SCHONBERG, J. A. & RALLISON, J. M. 1989 The lubrication force between two viscous drops. *Phys. Fluids* A 1, 77–81.

DAVIS, R. H., SERAYSSOL, J.-M. & HINCH, E. J. 1986 The elastohydrodynamic collision of two spheres. *J. Fluid Mech.* **163**, 479–497.

DERJAGUIN, B. & KUSSAKOV, M. 1939 Anomalous properties of thin poly-molecular films. *Acta Physicochim. URSS* **10**, 25–30.

DIMITROV, D. S. & IVANOF, I. B. 1978 Hydrodynamics of thin liquid films. On the rate of thinning of microscopic films with deformable interfaces. *J. Colloid. Interface Sci.* **64**, 97–106.

FRANKEL, S. P. & MYSELS, K. J. 1962 On the dimpling during the approach of two interfaces. *J. Phys. Chem.* **66**, 190–191.

HARTLAND, S. 1967 The approach of a liquid drop to a flat plate. *Chem. Engng Sci.* **22**, 1675–1687.

HARTLAND, S. 1969 The profile of a draining film beneath a liquid drop approaching a plane interface. *Chem. Engng Prog. Symp. Ser.* (91) **65**, 82–87.

HARTLAND, S. & ROBINSON, J. D. 1977 A model for an axisymmetric dimpled draining film. *J. Colloid. Interface* **60**, 72–81.

JONES, A. F., WILSON, S. D. R. 1978 The film drainage problem in droplet coalescence. *J. Fluid Mech.* **87**, 263–288.

LAMB, H. 1932 *Hydrodynamics*. Cambridge University Press.

LIN, C. Y. & SLATTERY, J. C. 1982 Thinning of a liquid film as a small drop or bubble approaches a solid plane. *AIChE J.* **28**, 147–156.

POZRIKIDIS, C. 1990 The deformation of a liquid drop moving normal to a plane wall. *J. Fluid Mech.* **215**, 331–363.

WACHOLDER, E. & WEIHS, D. 1972 Slow motion of a fluid sphere in the vicinity of another sphere or a plane boundary. *Chem. Engng Sci.* **27**, 1817–1828.